
Chapter 9: Understanding and Attributing Climate Change

Coordinating Lead Authors: Gabi Hegerl, Francis Zwiers

Lead Authors: Pascale Braconnot, Nathan Gillett, Yong Luo, Jose Marengo, Neville Nicholls, Joyce Penner, Peter Stott

Contributing Authors: M. Allen, C. Ammann, N. Andronova, R. Betts, A. Clement, W. Collins, S. Crooks, T. Delworth, R. van Dorland, C. Forest, P. Forster, H. Goosse, J. Gregory, D. Harvey, F. Joos, G. Jones, J. Kenyon, J. Kettleborough, V. Kharin, R. Knutti, H. Lambert, M. Lavine, T. Lee, D. Levinson, V. Masson, T. Nozawa, B. Otto-Bliesner, D. Pierce, S. Power, D. Rind, L. Rotstayn, B. D. Santer, C. Senior, D. Sexton, S. Stark, D. Stone, S. Tett, P. Thorne, M. Wang, B. Wielicki, T. Wong, L. Xu, X. Zhang, E. Zorita

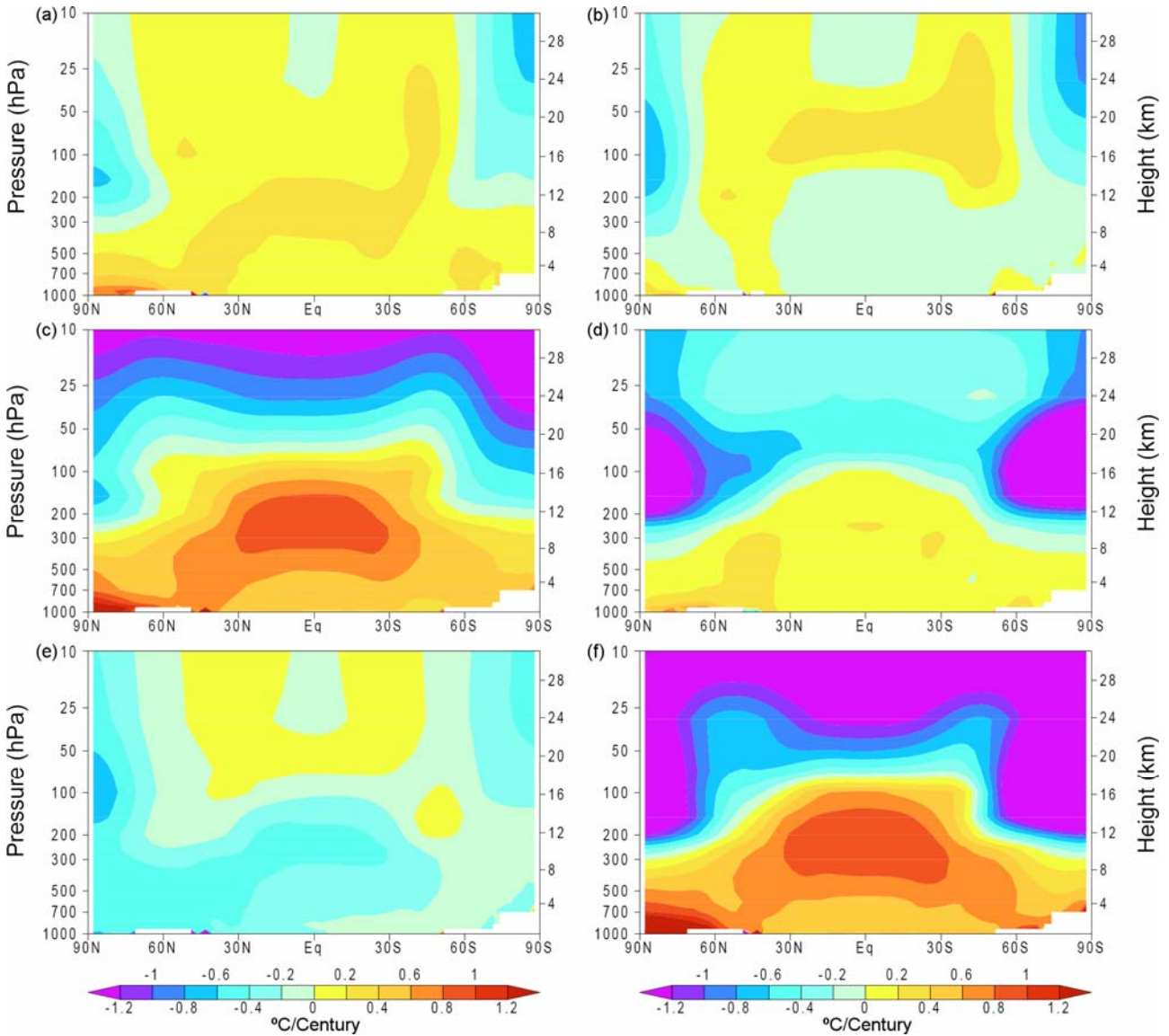
Review Editors: David Karoly, Laban Ogallo, Serge Planton

Date of Draft: 7 March 2006

Notes: TSU compiled version

1
2

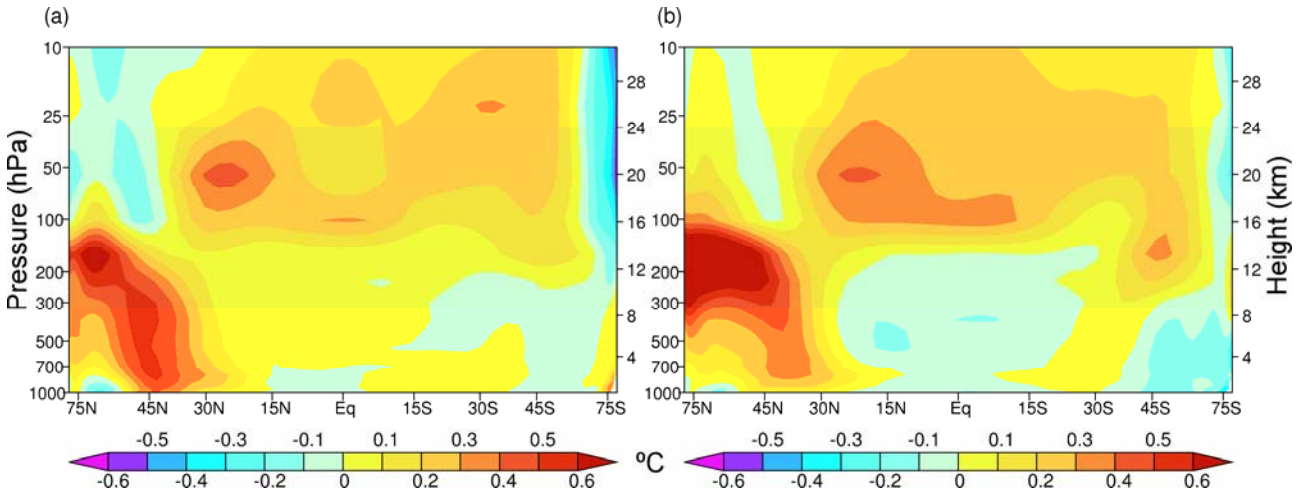
Figures



3
4
5
6
7
8
9
10
11

Figure 9.2.1. Zonal mean atmospheric temperature change during the 20th century ($^{\circ}\text{C}/\text{Century}$) as simulated by the PCM model from (a) solar forcing, (b) volcanoes, (c) well-mixed greenhouse gases, (d) tropospheric and stratospheric ozone changes, (e) direct sulphate aerosol forcing, and (f) the sum of all forcings. Plot is from 1000 hPa to 10 hPa (shown on left scale) and from 0 km to 30 km (shown on right). Based on Santer et al. (2003a).

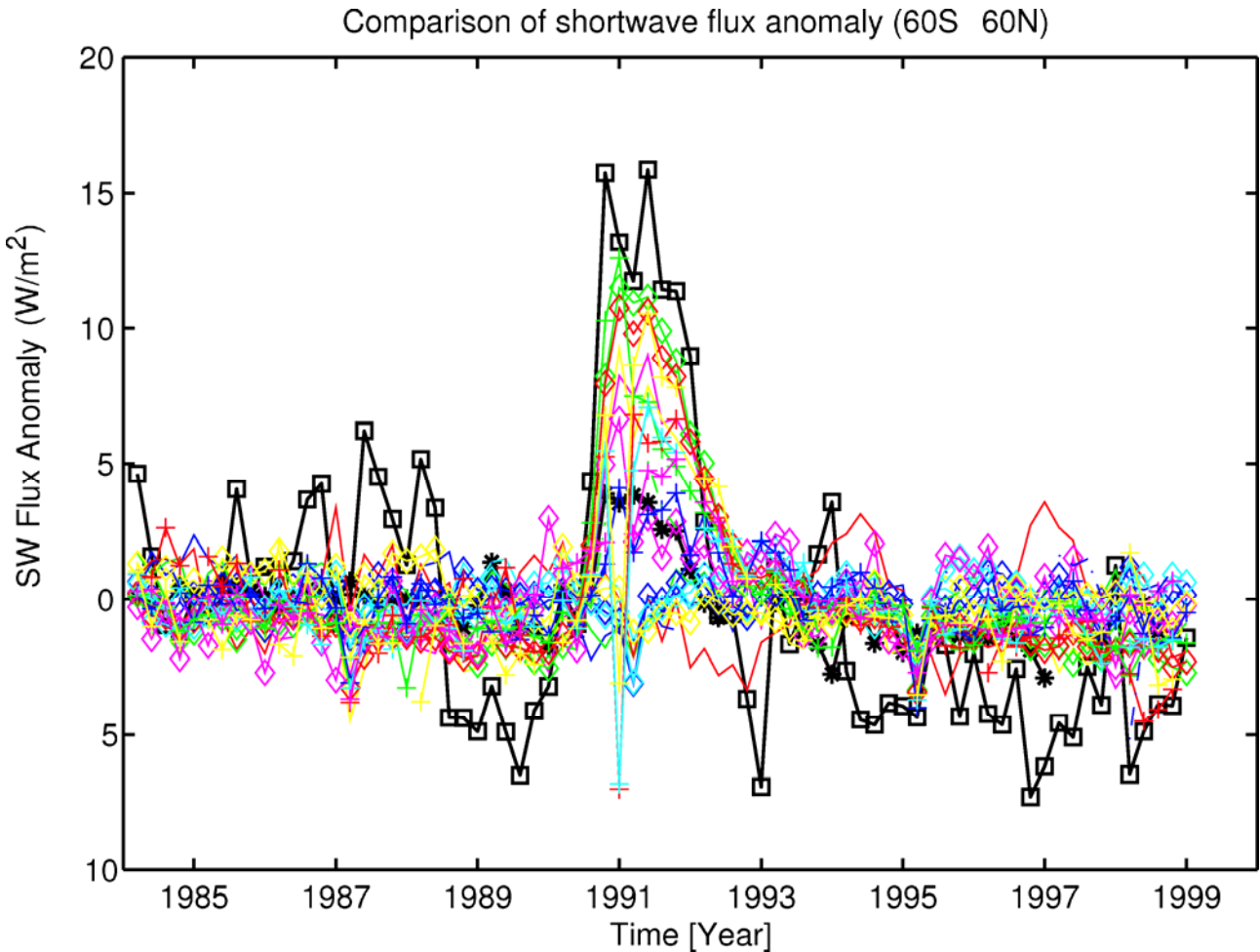
1
2



3
4
5
6
7
8
9
10

Figure 9.2.2. The zonal mean equilibrium temperature change (°C) between a present-day minus a preindustrial simulation of the CSIRO atmospheric model coupled to a q-flux ocean model from (a) direct forcing from fossil fuel black carbon and organic matter (BC+OM) and (b) the sum of fossil fuel BC+OM and biomass burning. . Plot is from 1000 hPa to 10 hPa (shown on left scale) and from 0 km to 30 km (shown on right). Note the difference in colour scale from Figure 9.2.1. Based on Penner et al. (2005)

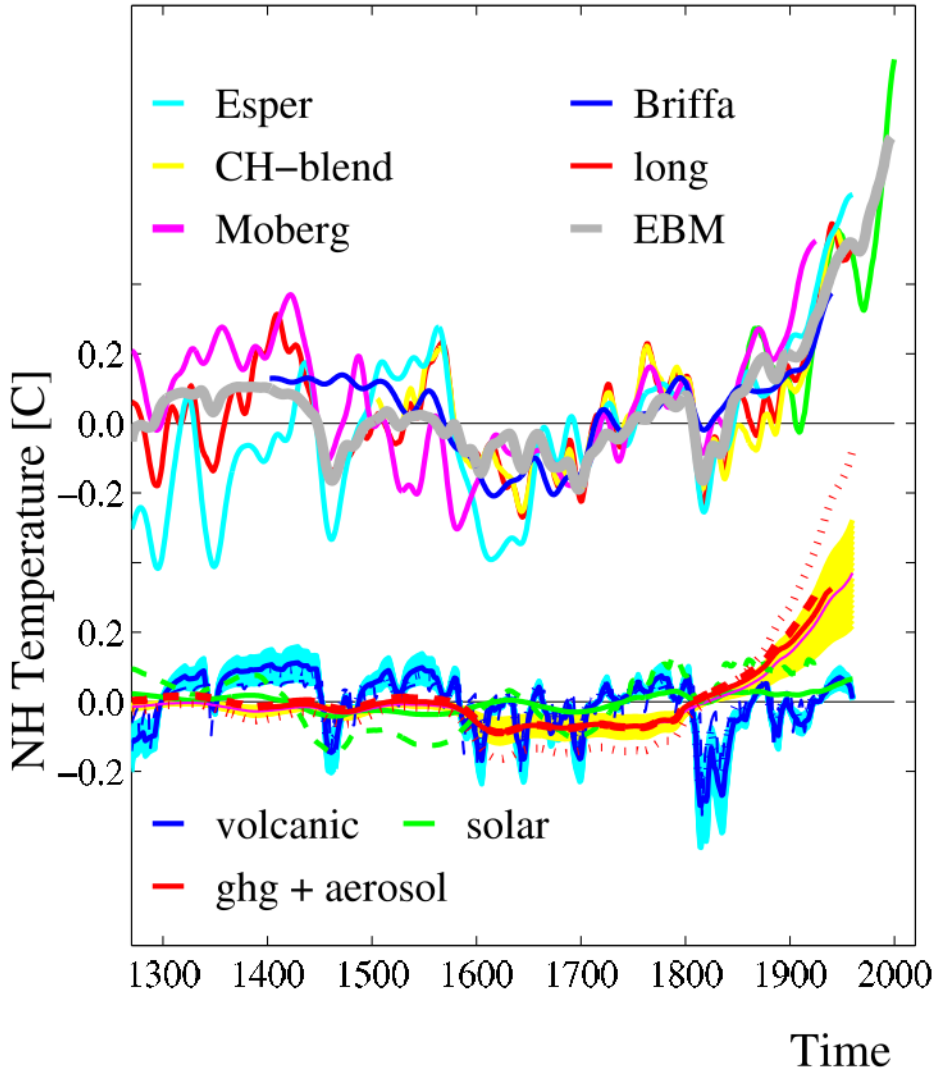
1
2



3
4
5
6
7
8
9
10
11
12
13

Figure 9.2.3. Comparison of outgoing shortwave flux anomalies (in W/m²) (calculated relative to the entire time period) from the IPCC AR4 models (coloured curves) with ERBS satellite data (black with stars; Wong et al., 2005) and with the ISCCP FD data set (black with squares, Zhang et al., 2004). Models shown are CCSM3, CGCM3.1(T47), CGCM3.1(T63), CNRM-CM3, CSIRO-MK3.0, FGOALS-g1.0, GFDL-CM2.0, GFDL-CM2.1, GISS-AOM, GISS-EH, GISS-ER, INM-CM3.0, IPSL-CM4, MRI-CGCM2.3.2 (model IDs 3-7, 10-17 and 20, Chapter 8, Table 8.2.1). The comparison is restricted to 60S-60N because the ERBS data are considered more accurate in this region. Note that not all models included the volcanic forcing from Pinatubo (1991–1993) and so do not predict the observed increase in outgoing solar radiation.

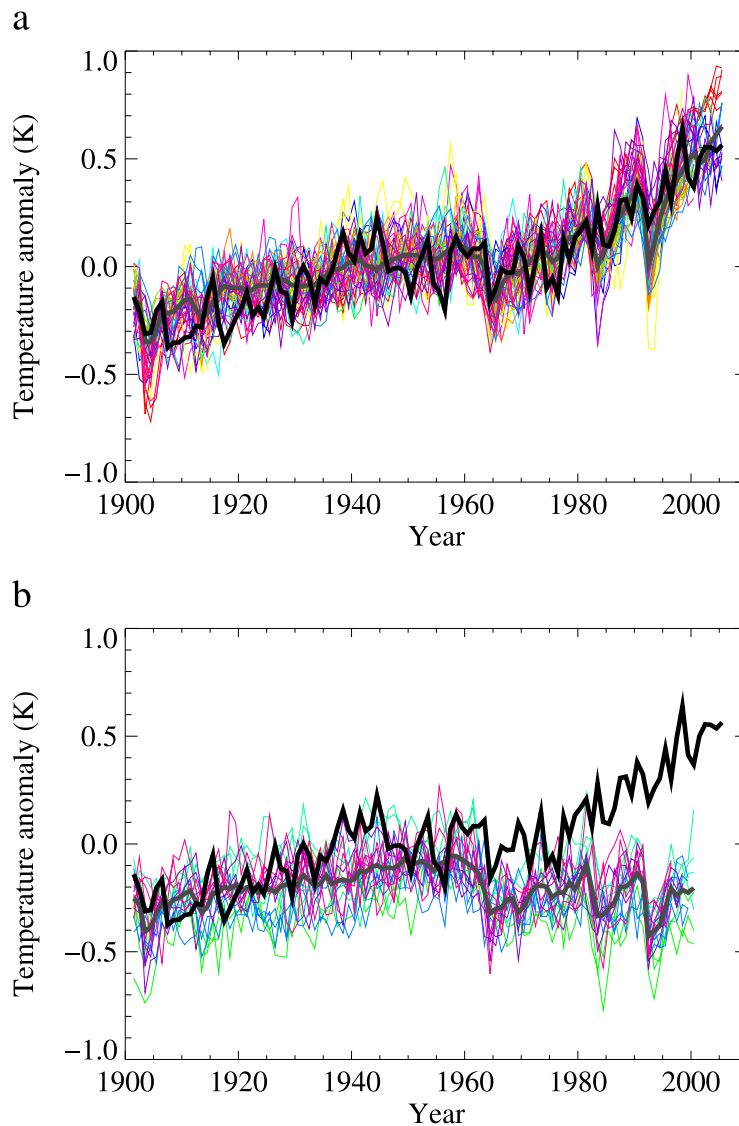
1
2



3
4
5
6
7
8
9
10
11
12
13
14
15
16
17
18
19

Figure 9.3.1. Contribution of external forcing to some high variance reconstructions of Northern Hemispheric temperature (reconstructions described in Table 9.3.1). The reconstruction by Esper et al. (2002) is calibrated to 30–90N land temperature, CH-blend and CH-blend (long) (Hegerl et al., 2006) to 30–90N mean temperature, and Moberg et al. (2005) to 0–90N temperature. NH 30–90N average temperature from an Energy Balance climate model (EBM) simulation forced with estimates of volcanic, solar, and anthropogenic forcing and a climate sensitivity 2.5°C is shown for comparison, instrumental data are shown by a green line. All top panel data are smoothed removing variance below 20 yrs, bottom panel data show fingerprints in the decadal time domain used for detection. The bottom panel shows an estimate of the contribution from individual forcings (volcanism, solar forcing, and greenhouse gas and aerosol forcing combined) and the associated 90% uncertainty range for detectable signals from the CH-blend (long) reconstruction. Best fit detectable fingerprints in the reconstructions by Briffa et al. (2001) (solid, fat), Esper (dotted), Moberg (dashed) and Ch-blend (solid, thin) are also shown. Note that only Moberg et al. contains a detectable solar signal, shown by a green dashed line. Forcing fingerprints are centered to the period analyzed. Hegerl et al. (2003) updated.

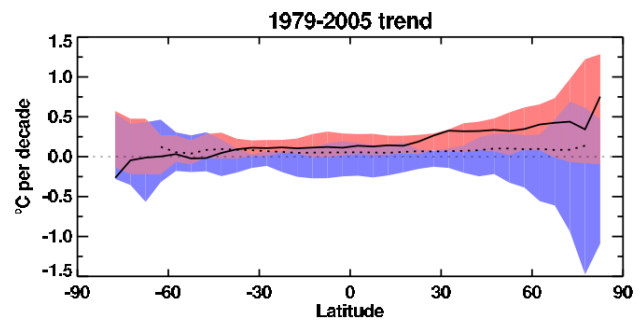
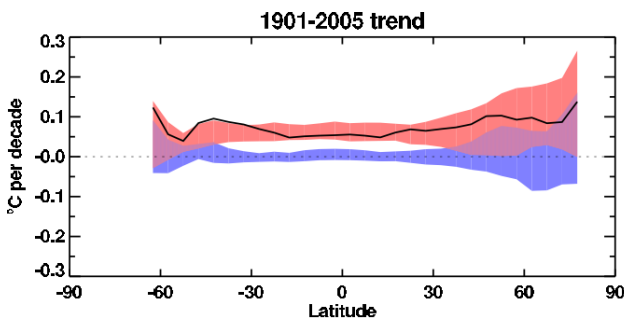
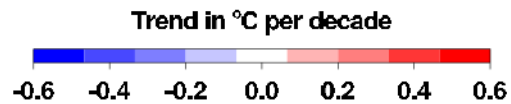
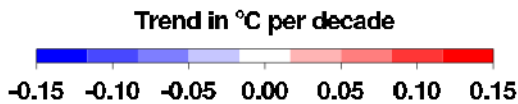
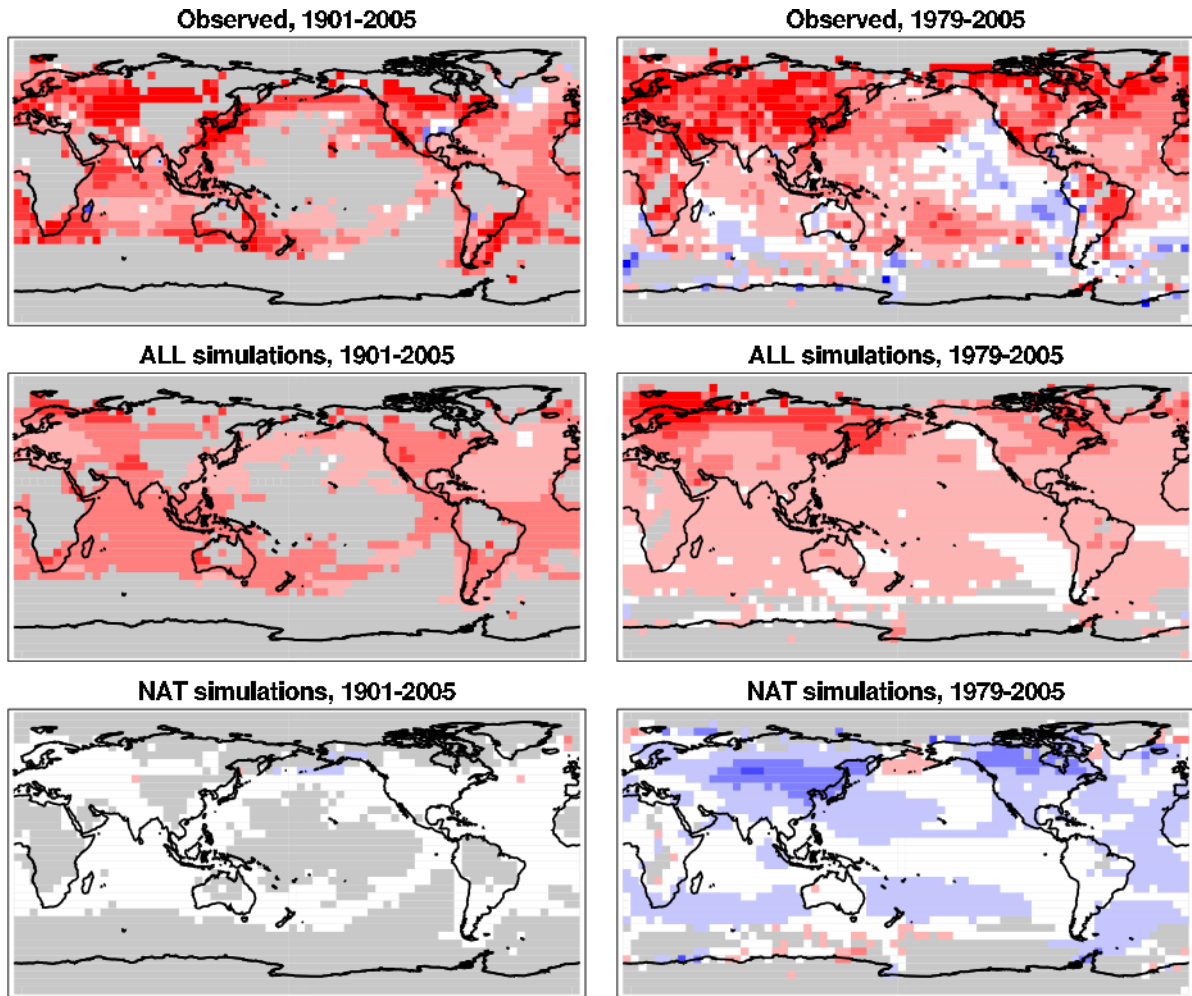
1



2
3

4 **Figure 9.4.1.** Global mean temperature anomalies, as observed (black line, HadCRUT2v, Parker et al., 2004)
 5 and as modelled by a range of climate models when the simulations include (a) both anthropogenic and
 6 natural forcings and (b) natural forcings only. The multimodel ensemble mean is shown in grey, and
 7 individual simulations are shown in colour, with curves of the same colour indicating different ensemble
 8 members for the same model. Thirteen models are included; 11 of which are described in Chapter 8, Table
 9 8.2.1 and are identified in the list below by their Model ID given in that table. An additional two models are
 10 not described in Chapter 8, Table 8.2.1; these are ECHAM4-OPYC3 (Stendel et al., 2006), and GFDL-R30
 11 (Delworth et al., 2002). The 51 model simulations shown that include both anthropogenic and natural
 12 forcings are: CCSM3 (model ID 3; 6 simulations), ECHO-G (9,3), GFDL-CM2.0 (11,3), GFDL-CM2.1
 13 (12,3), GFDL-R30 (A2, 3), 6: GISS-EH (14,5), 7: GISS-ER (15,9), 8: INM-CM3.0 (16,1), 9:
 14 MIROC3.2(medres) (19,4), 10: MRI-CGCM2.3.2 (20,5), 11: PCM (21,4), 12: HadCM3 (22,4). The 19
 15 model simulations shown that include natural forcings only are: ECHO-G (model ID 9, 3 simulations),
 16 MIROC3.2(medres) (19,4), MRI-CGCM2.3.2 (20,4), PCM (21,4), HadCM3 (22,4). The observed and
 17 simulated timeseries in (a) are expressed as anomalies relative to the 1901–1997 mean. The simulations in (b)
 18 are expressed as anomalies relative to the corresponding model simulation that also includes anthropogenic
 19 forcing. Only models whose control simulations have a trend of less than 0.2°C/century are included in this
 20 figure. Each simulation was sampled so that coverage corresponds to that of the observations, and was
 21 centered relative to the 1901–1997 mean obtained by that simulation. The “ALL” simulations were extended
 22 to 2005 by adding their SRES A1B continuation runs where available. Where not available, and in the case
 23 of the NAT simulations, the mean for the 1996–2005 decade was estimated using model output from 1996 to
 24 the end of the available runs. Observations were centered relative to the same period. After Stott et al.
 25 (2006c).

1
2



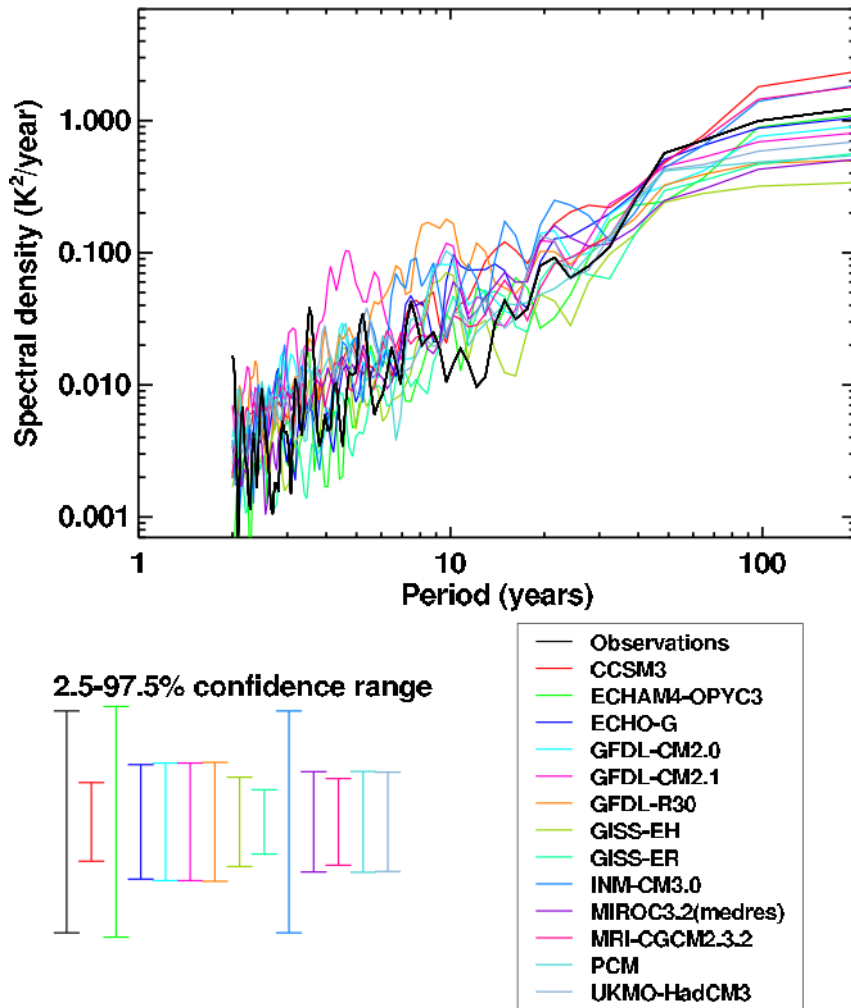
3
4

5

6 **Figure 9.4.2.** Trends in observed and simulated temperature changes over the 1901–2005 (left column) and
 7 1979–2005 (right column) periods. Note scales are different between columns. The “ALL” simulations were
 8 extended to 2005 by adding their SRES A1B continuation runs where available. Where not available, and in
 9 the case of the NAT simulations, the mean for the 1996–2005 decade was estimated using model output
 10 from 1996 to the end of the available runs. First row: trends in observed temperature changes (HadCRUT2v,
 11 Parker et al., 2004). Second row: average trends in 51 historical simulations from 13 climate models
 12 including both anthropogenic and natural forcings. Third row: average trends in 19 historical simulations
 13 from 5 climate models including natural forcings only. Fourth row: average trends for each latitude;
 14 observed trends are indicated by solid black curves; red shading indicates the 5th to 95th percentiles of trend
 15 estimates from the 51 simulations including both anthropogenic and natural forcings; blue shading indicates
 16 the 5th to 95th percentiles of trend estimates from the 19 simulations with natural forcings only; for
 17 comparison, the dotted black curve in the right hand plot shows the observed 1901–2005 trend.

1 Error!

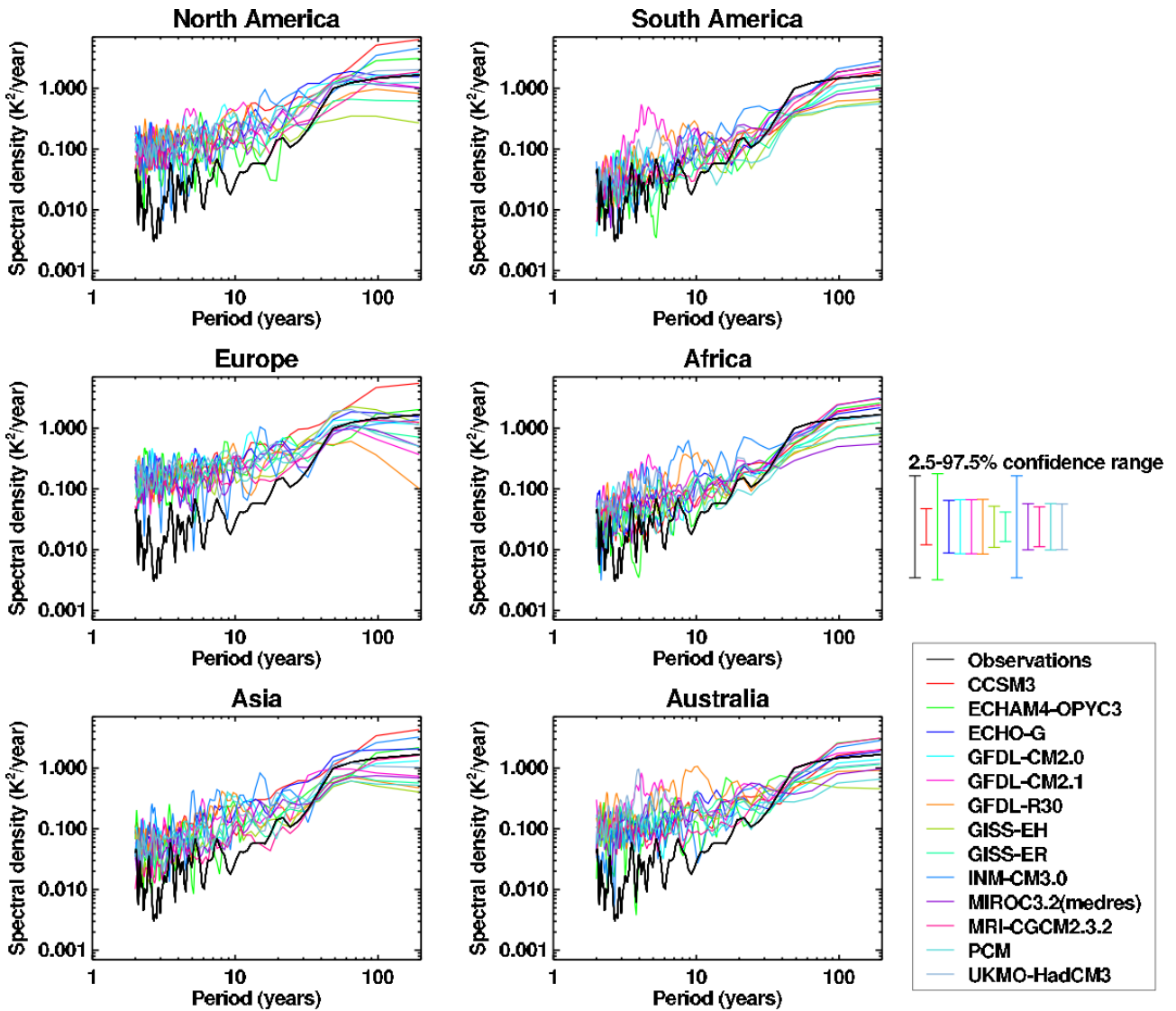
2



3
4
5
6
7
8
9
10
11

Figure 9.4.3. Power spectra of annual mean global mean temperatures from the observed record (HadCRUT2v, Parker et al., 2004) and from coupled GCMs including both anthropogenic and natural forcings. All spectra are estimated using a Tukey-Hanning filter of width 97 years. The model spectra displayed are the averages of the individual spectra estimated from individual ensemble members. The same 51 simulations and 13 models are used as in Figure 9.4.1. All models simulate variability on decadal timescales and longer that is consistent with observations at the 5% significance level, and all models, but one, are consistent at the 10% level.

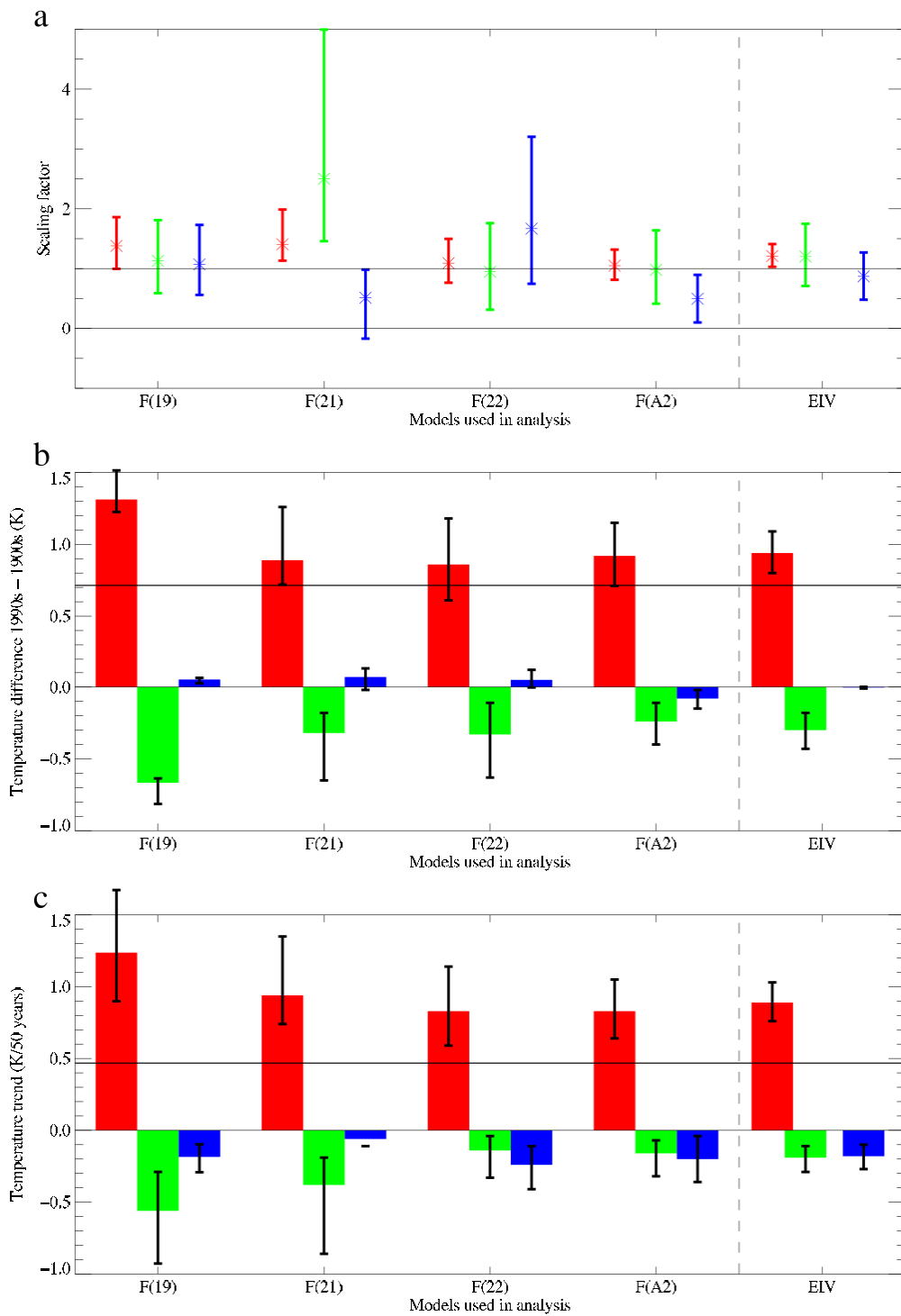
1
2



3
4
5
6
7
8
9
10
11
12
13

Figure 9.4.4: As Figure 9.4.3, except for continental mean temperature for continental regions defined by combining two or more sub-continental regions (defined in Figure 11.3.1.1, see also Giorgi and Francisco, 2000). The continents are North America (ALA, CGI, WNA, CNA, ENA), Europe (NEU, SEU), Asia (NAS, CAS, TIB, EAS, SAS, SEA), South America (CAM, AMZ, SSA), Africa (SAH, WAF, EAF, SAF), and Australia (NAU, SAU). Models simulate variability on decadal timescales and longer that is consistent with observations in all cases except for 2 models over North America (at the 10% and 5% significance levels), 2 models over South America (at the 10% significance level, but not the 5% significance level), and one model over Europe (at the 10% and 5% significance levels).

1

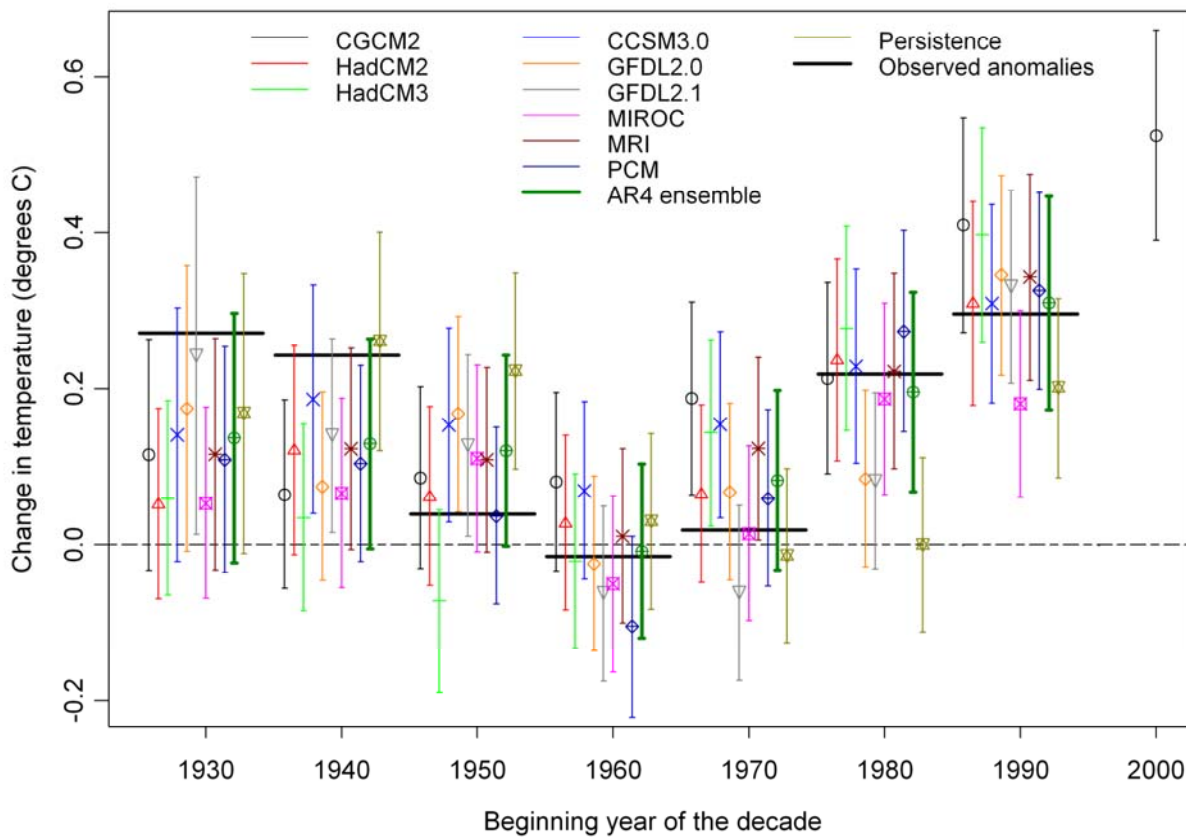


2
3

4 **Figure 9.4.5.** 5 to 95 percentile uncertainty limits on scaling factors (a), reconstructed temperature changes
 5 over the 20th century (b), expressed as difference between 1990–1999 mean temperature and 1900–1909
 6 mean temperature and reconstructed temperature trends over 1950–1999 (c) for the greenhouse gas (red),
 7 other anthropogenic (green), and natural (blue) components, based on optimal detection analyses. Where
 8 only dark blue bars are shown, this refers to the total natural component and where dark blue and light blue
 9 bars are shown they refer to volcanic and solar contributions respectively. Labeled by F are the results of
 10 full time-space optimal detection analyses (Nozawa et al., 2005; Stott et al., 2006c) using a total least squares
 11 algorithm (Allen and Stott, 2003) from ensembles of simulations containing each set of forcings separately
 12 (where the numbers refer to the model ID as listed in Chapter 8, Table 8.2.1 and the caption to Figure 9.4.1).
 13 Labeled by EIV is an optimal detection analysis which combines spatio-temporal patterns of response from
 14 three models for each of the three forcings separately and incorporates inter-model uncertainty (model IDs
 15 21, 22, and GFDL-R30, Huntingford et al., 2006).

1
2

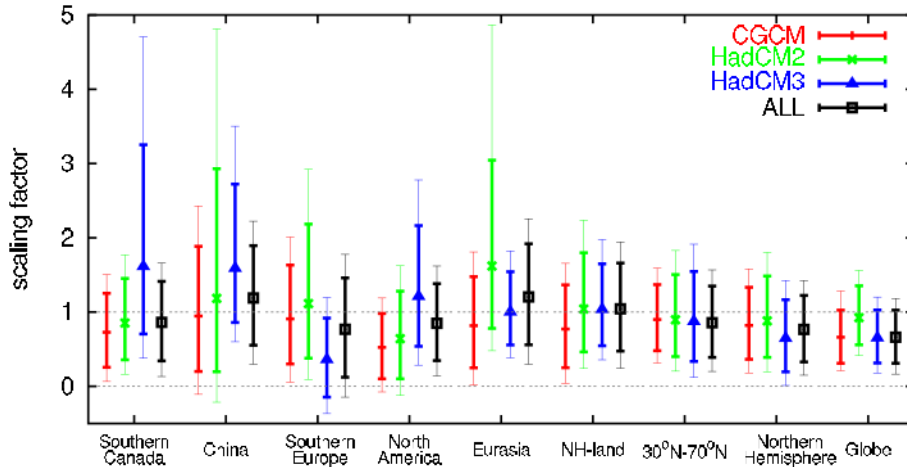
Change in global mean temperature relative to the previous 3 decades



3
4
5
6
7
8
9
10
11
12
13
14
15
16
17
18

Figure 9.4.6. Hindcasts and their 5–95% confidence bounds of global decadal mean surface temperature anomalies relative to the preceding 30-year climatology made with CGCM2, HadCM2 (see Chapter 8, Table 8.1, IPCC, 2001) and HadCM3 (model ID 22, Chapter 8, Table 8.2.1) simulations of the 20th century using anthropogenic forcing only (left hand column of legend) and with simulations from several models participating in IPCC AR4 C20C3M that use anthropogenic and natural forcings (center column of legend; model IDs 3, 11, 12, 19, 20, 21, Chapter 8, Table 8.2.1). Hindcasts based on the ensemble mean of the selected C20C3M models are indicated by the thick green line. Observed decadal anomalies relative to the previous three decades are indicated by horizontal black bars. A hindcast that persists anomalies from the previous decade is also indicated. The hindcasts agree well with observations from the 1950’s onwards. Hindcasts for the decades of the 1930’s and 1940’s are sensitive to the details of the hindcast procedure. A forecast for the decadal global mean anomaly for the decade 2000–2009, relative to the 1970–1999 climatology, based on simulations performed with the CCCma CGCM2 model is also displayed. Units are °C. From Lee et al. (2006).

1
2



3
4
5
6
7
8
9
10
11
12
13
14
15
16
17
18

Figure 9.4.7. Scaling factors indicating the match between observed and simulated decadal near surface air temperature change (1950–1999) when greenhouse gas and aerosol forcing responses (GS) are taken into account in optimal detection analyses on a range of spatial scales. Thick bars indicate 90% confidence intervals on the scaling factors, and the thin extensions indicate the increased width of these confidence intervals when estimates of the variance due to internal variability are doubled. Scaling factors and uncertainties are provided for different spatial domains including: Southern Canada (Canadian land area south of 70°N), China, Southern Europe (European land area bounded by 10°W–40°E, 35°–50°N), North America (North American land area between 30°N–70°N), Eurasia (Eurasian land area between 30°N–70°N), mid-latitude land area between 30°N–70°N (labelled NH-land), the Northern Hemisphere mid-latitudes (30°N–70°N including land and ocean), the Northern Hemisphere, and the Globe. The GS signals are obtained from CGCM1 and CGCM2 combined (labeled CGCM, see Chapter 8, Table 8.1, IPCC, 2001), HadCM2 (see Chapter 8, Table 8.1, IPCC, 2001), and HadCM3 (model ID 22, Chapter 8, Table 8.2.1), and these 4 models combined (labeled ALL). After Zhang et al. (2006); Hegerl et al. (2005).